

Chapter I

Introduction

Overview of the chapter:

In this chapter, a brief review of the fundamental characteristics of CdSe nanocrystals is given, including the crystalline structure and the electronic structure. The major issues in this thesis research are introduced.

1.1 Major Issues of the study on CdSe nanocrystals

Nanocrystals (NCs) and quantum dots (QDs) are low-dimensional materials composed of atoms numbering from several tens to thousands. When the material size approaches the nano-regime, two factors play dominant roles in their physical properties. One is the size effect: NCs have unique properties associated with the spatial confinement of the electronic excitations and, in particular, possess discrete electronic states, in contrast to the bulk band structure, with an effective band gap blue shifted from that of the bulk [1,2]; the other is the surface effect: NCs are also characterized by their large ratio of the surface atom to volume atom. For example, a CdSe NC with the diameter of 18

Å (42 Å) has about 109 atoms (346 atoms) and roughly 55% (25%) of its atoms at the surface. Both the quantum size and the surface effects result in variously distinct properties in NCs from the bulk.

Much of experimental and theoretical research concentrated on CdSe NCs, which can be regarded as prototypical nano semiconductor. In the beginning of 1990s, C. B. Murray *et al.* developed a simple synthetic method, based on the pyrolysis of organometallic reagents by injection into a hot coordinating solvent, to produce the nanometer-size CdSe crystallites of high quality and narrow size distribution [3]. The organic molecules used in this preparation can provide a high dispersibility in hydrocarbon solvents and surface stabilization for NCs. Subsequently, some modified approaches [4,5] were applied in the production of highly luminescent CdSe NCs using inorganic passivation (quantum yield of ~85%). Recently, various shapes of CdSe NCs, such as rod, arrow, teardrop, and branched tetrapod, have been achieved by controlling the synthetic conditions [6,7].

The NCs and QDs are of great interest in scientific research and technological applications due to a strong correlation between their size and their electronic behavior [8-10]. Stable, controllable, and monodispersed NCs offer an opportunity to explore the dimensionally dependent characteristics of materials, such as optical properties, surface effect, as well as crystalline order [11-14]. By taking advantage of the unique physical and chemical properties of NCs, they have been used to develop light-emitting diodes [15,16], biosensors [17,18], catalysis [19], and solar cells [20].

Until now, a number of the realistic nature and the physical mechanism in these fine crystallites have not been fully clarified. In this thesis, our study is

motivated by the strong dependence of structural and electronic behaviors on particle size for CdSe NCs. We focus our study on NCs with the particle size (mean diameters) in the range 18–42 Å, which is smaller than the bulk exciton radius of 55 Å, in the strong confinement regime. Synchrotron radiation is a powerful tool to study nanometer-size materials, because of its distinct advantages from conventional X-ray source. By means of synchrotron experimental techniques, the structural and electronic properties of CdSe NCs can systematically be investigated and discussed in detail; we found that the size-dependent behaviors are associated with the surface passivation of NCs, providing an understanding on basic science and technical applicability.

An introduction of fundamental knowledge about crystalline structure and electronic characteristics of CdSe NCs and an outline of the thesis are given in the following sections.

1.2 Wurtzite and zinc-blende structures

Wurtzite (WZ) and zinc blende (ZB) are the most common crystal structures of II-IV semiconductors (e.g. CdSe, CdS, and ZnSe). The WZ structure has a hexagonal unit cell with two lattice parameters a and c . In ideal case, the ratio $c/a = \sqrt{8/3} = 1.633$ [21]. As shown in Fig. 1.1, this structure is composed of two hexagonal close-packed sublattices, which are shifted with respect to each other along the three-fold c axis by the amount of u in fractional coordinates. Ideally $u = 3/8$. Both sublattices are occupied by one atomic species only, resulting in four atoms per unit cell. Locally, every atom of one kind is surrounded by four atoms of the other kind which are positioned at the edges of a tetrahedron

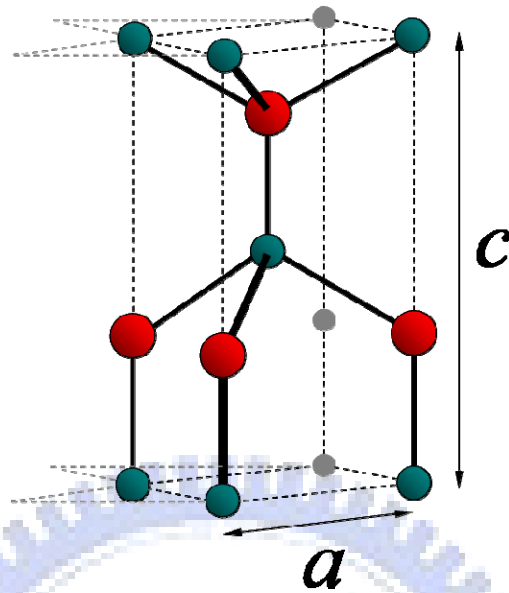


FIG. 1.1: Scheme of a unit cell of wurzite structure.

(coordination number 4). The symmetry of the WZ structure is given by space group $P6_3mc$, and the positions of two inequivalent atoms are $(\frac{1}{3}, \frac{2}{3}, 0)$ and $(\frac{1}{3}, \frac{2}{3}, u)$. Table 1.1 represents the structural parameters of wurzite [22] compared to the ideal values.

Table 1.1 Structural parameters of CdSe and ideal wurzite [22].

	CdSe	Ideal wurzite
$a(\text{\AA})$	4.299	
$c(\text{\AA})$	7.010	
c/a	1.631	1.633
u	0.376	0.375

The ZB structure belongs to space group $F\bar{4}3m$ and consists of two interpenetrating and identically oriented fcc lattices offset from one another by one-quarter of a body diagonal as shown in Fig. 1.2. There are four atoms per unit cell, the coordinates of one atom type being $(0,0,0)$, $(0, \frac{1}{2}, \frac{1}{2})$, $(\frac{1}{2}, 0, \frac{1}{2})$, $(\frac{1}{2}, \frac{1}{2}, 0)$, and those of the other type being $(\frac{1}{4}, \frac{1}{4}, \frac{1}{4})$, $(\frac{1}{4}, \frac{3}{4}, \frac{3}{4})$, $(\frac{3}{4}, \frac{1}{4}, \frac{3}{4})$, $(\frac{3}{4}, \frac{3}{4}, \frac{1}{4})$, in units of a conventional cubic cell. As a result, each atom of one kind is surrounded by four atoms of the other kind forming a regular tetrahedron (coordination number 4). The overall equivalent bond length is equivalent to $R = (\sqrt{3}/4)a$.

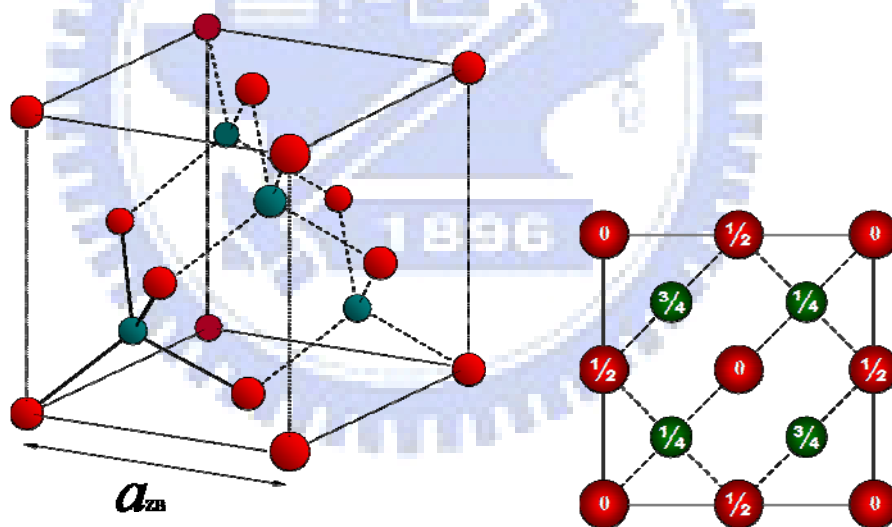


FIG. 1.2: Crystal structure of zinc-blende structure and atomic positions in the cubic cell of the zinc-blende structure projected on a cube face [23]. Fractions denote height above the base in units of a cube edge.

Both WZ and ZB structures are the tetrahedral coordination, the short range order of these structures is therefore virtually identical. If we ignore slight deviations from ideal spherical closed packing in the WZ structure, each atom is

tetrahedrally surrounded by four nearest neighbors with the same bond distance as in the ZB modification. Also the twelve next-nearest neighbors are at the

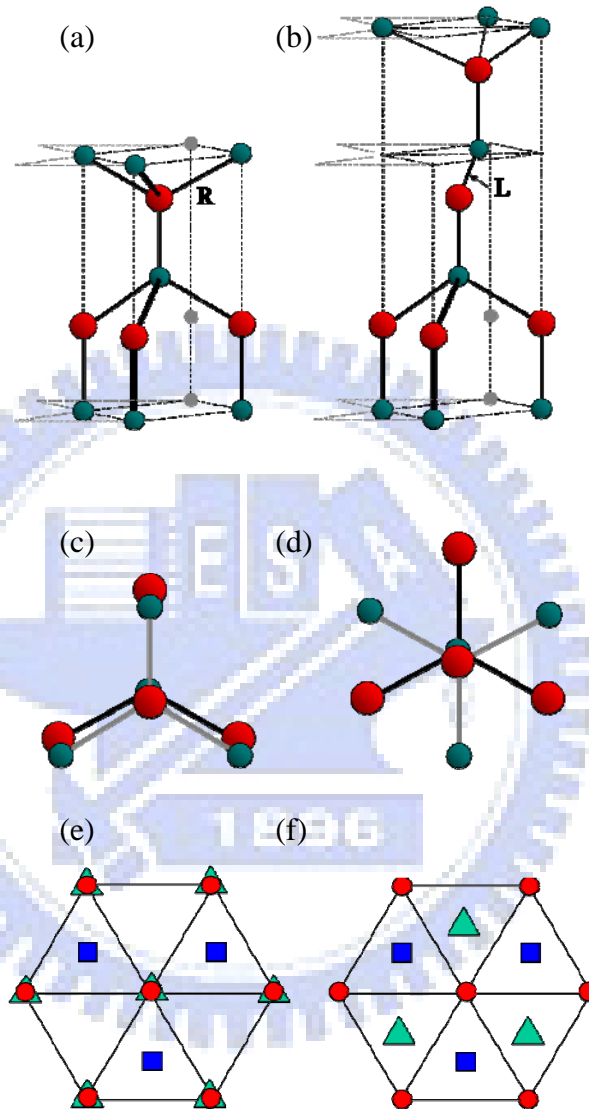


FIG 1.3: Three views of the difference between the wurtzite and zinc-blende crystal structures [24]. (a) and (b) show the handedness of the fourth interatomic bond along the right (R) for wurtzite and left (L) for zinc blende. (c) and (d) show the “eclipsed” and “staggered” dihedral conformations for wurtzite and zinc blend. (e) and (f) show the layer stacking along (111).

same distance in both structures. Significant difference is found only for the

third next-nearest neighbors. This difference can simply be described by regarding the handedness of the fourth interatomic bond along the $\langle 111 \rangle$ closed packed chain corresponding to the third nearest neighbor relation in both structures (Fig. 1.3). In the ZB structure, triangularly arranged atoms in the closed-packed $\{111\}$ plane are in “staggered” configuration with the triangularly arranged unlike atoms in third nearest neighbor distance, that is, the latter are rotated around an angle of 60° with respect to the former (Fig. 1.3). In contrast, triangularly arranged atoms in the $\{0001\}$ closed packed basal plane are in an “eclipsed” (i.e., identical) configuration in the WZ structure. Taking these different arrangements in closed-packed planes as the building principle for both crystal structures, one finally ends up with the following stacking sequences:

...ABABABABAB...

for the WZ, and

...ABCABCABCABC...

for the ZB type, which completely characterize both structure types as shown in Fig. 1.3. A fault in the stacking sequence transforms one structure into the other. Hence, the respective stacking fault energy corresponds to the free energy difference between the WZ and ZB modifications.

1.3 Electronic structure of CdSe nanocrystals

A system of electrons fully confined in all three dimensions has a series of discrete electronic states, as do atoms and molecules. Semiconductor NCs, with the tunability of their electronic and optical properties, have attracted considerable interest as technologically important materials. Hence, the study of

the quantum confinement in these semiconductors has been a subject of intense study. Though the first approach to obtain a quantitative understanding of the quantum confinement effects on the band gap of the NC as a function of size was given by the effective mass approximation [25], it is well known to overestimate the band gap in the small size regime. Typical absorption spectrum of CdSe NCs and the energy level diagram based on elementary theory [25] are shown in Fig. 1.4. In the past few decades, the theoretical predictability of the variation of band gap as a function of size has substantially improved due to the development of a host of different theoretical approaches, starting from the *ab initio* methods [26] to the semiempirical pseudopotential [27,28] and tight binding [29] approaches. Two theoretical methods are introduced as follows.

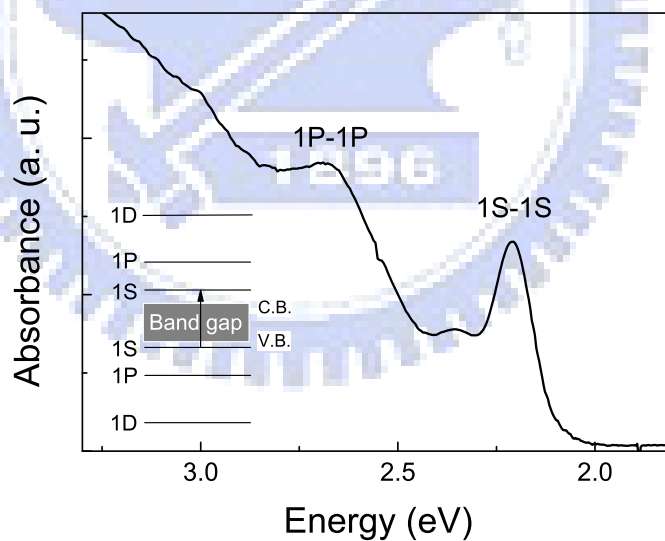


FIG. 1.4: Absorption spectrum of CdSe nanoparticles with size of 33 Å. Inset: Energy level diagram for a spherical cluster from elementary theory [25].

1.3.1 Effective-mass model

When a semiconductor crystal absorbs the incident light, an electron at the top of the valence band can be excited to the bottom of the conduction band. Using the techniques of quantum-field theory, one may replace this interacting many-body quantum problem by a two-body problem consisting of an electron in the conduction band and a hole (absence of an electron) in the valence band. The electron and the hole interact with the lattice, as well as with each other. To a good approximation the wave functions of the electron and hole are plane waves with masses m_e and m_h , respectively, in units of the free-electron mass m_0 [$m_e=0.13$ and $m_h=0.45$ for CdSe (Ref. 30)]. The effect of the interaction of the electron and hole with the periodic potential of the lattice is such that m_e and m_h are usually less than m_0 . In other words, the effect of the periodic potential on the electrons is subsumed in their effective masses. This is the effective-mass model.

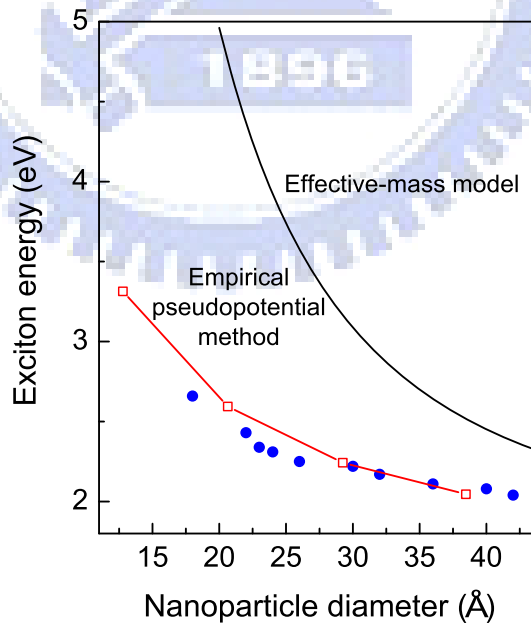


FIG. 1.5: Lowest transition energy of CdSe nanoparticles as a function of size, obtained from the absorption experiments, compared with the prediction of the effective mass approximation [31,32] and the empirical pseudopotential method [33] both including Coulomb term.

If the cluster is a sphere, the allowed wave vectors of the lowest exciton state are given by $k=\pi/R$ and the effective-mass model [31,32] gives the exciton energy as:

$$E_x = E_g(\text{bulk}) + \frac{\hbar^2 \pi^2}{2R^2} \left(\frac{1}{m_e} + \frac{1}{m_h} \right) - \frac{1.786}{\varepsilon R} - 0.248 E_{Ry} \quad (1.1)$$

where $E_g(\text{bulk})$ is the band gap of bulk crystal [1.74eV for CdSe (Ref. 30)], R is the radius of the cluster, ε is the dielectric constant, and $E_{Ry} = \mu e^4 / (2\varepsilon^2 \hbar^2)$ is the effective Rydberg energy of a bulk exciton, μ being the reduced mass of the electron-hole pair [32]. The second, third, and fourth terms in Eq. (1.1) give kinetic, Coulomb, and correlation energies of the electron-hole pair, respectively, in atomic units. Figure 1.5 shows the energy of first absorption peak (lowest 1S–1S transition) for CdSe NCs as a function of size compared with the theoretical calculation. We note that this relation is valid for NCs of small size in the strong confinement regime, in which the electron and hole are bound individually by the NC surface, in contrast to those of larger size in the weak confinement regime and bulk, where the electron-hole pair is bound by hydrogenic-like Coulomb attraction.

1.3.2 Empirical pseudopotential method

The energies of the electronic states in a crystal or cluster are determined by the Schrödinger equation:

$$H\psi_{n,k}(r) = E_n(k)\psi_{n,k}(r), \quad (1.2)$$

where H is the Hamiltonian, $\psi_{n,k}$ are its wave functions, $E_{n,k}$ are the corresponding eigenvalues, k are the wave-vector quantum numbers of the wave

functions, and n are the band indices. It is impossible to solve this equation exactly for the large clusters, which typically contain thousands of electrons. Consequently, several approximations are made to formulate this many-body problem into a numerically tractable form. First, the electrons in the inner orbits are assigned to the nuclei to obtain charged cores. Second, the Born-Oppenheimer approximation is imposed to clamp the cores to fixed lattice sites. Third, each valence electron is assumed to move independently in the mean field of the fixed cores and other valence electrons. With these approximations the exact crystal-field potential experienced by the valence electrons is replaced by an effective potential (pseudopotential) $V_p(r)$ to obtain the valence-electron Hamiltonian:

$$H = -\frac{\hbar^2}{2m}\nabla^2 + V_p(r). \quad (1.3)$$

There are numerous techniques for determining these pseudopotentials. Among these, the empirical pseudopotential method has proved to be an elegant and simple means of obtaining the electronic energy levels (band structures or dispersion curves) of semiconductor crystals with reasonable accuracy [34].

Since $V_p(r)$ has contributions from all the atoms in the crystal, it is given by

$$V_p(r) = \sum_{R,j} v_j(r - R - d_j), \quad (1.4)$$

where v_j is the atomic pseudopotential of the j th basis atom at a lattice site R , d_j is the position vector of the j th basis atom relative to R , and the summation is over all lattice sites and all the basis atoms j at each lattice site.

Wang and Zunger [33] performed the semiempirical pseudopotential calculation for electronic structure of CdSe QDs with up to 1000 atoms, as shown in Fig. 1.5. The calculated exciton energies agree very well with our experimental results for the range of nanoparticle size we have studied.

1.4 Framework of the thesis

In **Chapter II**, we will introduce the fundamental principles and approaches of experiments, including the sample preparation, optical measurements, powder X-ray diffraction (XRD), extended X-ray absorption fine structure (EXAFS), and photoemission spectroscopy (PES).

In **Chapter III**, we have quantitatively investigated the size dependence of the distinct bond length in CdSe NCs with the use of powder XRD and EXAFS. The correlation between size and structure has attracted much attention in the past decades. The combination of powder XRD studies and transmission electron microscope (TEM) imaging yields a description of average CdSe NC structure, including the lattice constant, crystallite size, aspect ratio, stacking fault density, and the amount of surface disorder [16]. A detailed EXAFS investigation shows the interior and surface properties of CdTe NCs, as well as a significantly enhanced static disorder both in particle core and surface [35]. The contraction in average bond length of NCs can be characterized by a simple liquid drop model [36], which was also found to be sensitive to the surface modification [37]. Here, our results indicate that the distortion in a tetrahedron structure of CdSe NCs is related to the surface tension influenced by organic passivation and the atomic relaxation due to stacking faults.

In **Chapter IV**, we carried out high-resolution photoemission experiments to explore the core level and valence band of CdSe NCs. The electronic properties of semiconductor NCs have a strong dependence on their size being comparable to or smaller than the bulk exciton diameter. Theoretical studies on such systems have predicted many interesting effects in the electronic structure of

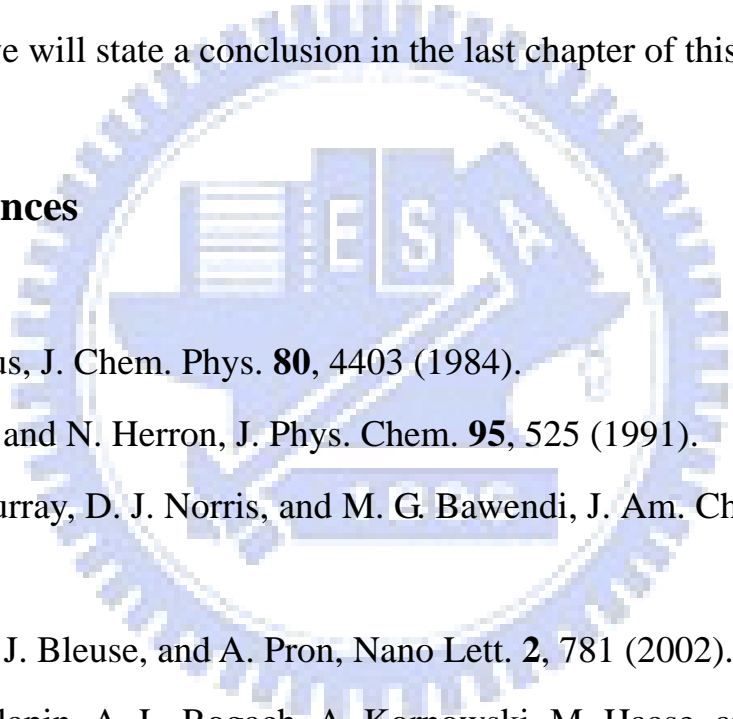
semiconductor NCs including discrete, well-defined states near the edges of the band [31,32]. Photoemission spectroscopy is known as a most direct method for contributing heavily to our understanding in the electronic structure of matter. Colvin *et al.* first applied valence-band photoemission to a QD system [38]. They attributed the valence-band shift to a combination of quantum confinement and photoemission final-state effect. More recently, the dynamic final-state effect depending on the cluster-substrate interaction was developed to describe the photoemission spectral features near the Fermi-level onset for Ag clusters [39]. Imamura *et al.* thus followed to discuss the passivant dependence of alkanethiolate-passivated Au nanoparticles [40]. Until now, however, the detailed investigation of electronic properties of semiconductor NCs using PES is still lacking. Here, we found that the core-level energy shift is due solely to photoemission final-state effect and, on the other hand, the quantum shift cannot be excluded in the shift of valence-band edge. The effect in the final state related to the interaction between a CdSe NC and its neighbors by changing the surfactants is also discussed, which can be elucidated by a dynamic model.

In **Chapter V**, we have investigated the size-dependent photoluminescence (PL) efficiency of CdSe NCs with two different growth rates and linked it to the surface properties studies by synchrotron PES. Various semiconductor NCs, such as CdSe [41], ZnS [42], InAs [43], and CdTe NCs [44], have been investigated their surface properties by PES. One can adapt the photoelectron escape depth for quantitatively estimating the surface thickness for core NCs and the inorganic capping layer thickness for core/shell systems [42,45]. The PL efficiency is dictated by surface/interface of NCs; the defect or the lone-pair orbital concentration at the surface enhances the probability of the nonradiative

recombination processes [11,46]. Although many related studies have been reported [44,46], the realistic nature of the exciton recombination via surface states still needs to be fully clarified. Combined with optical spectroscopy and PES, the correlation between PL efficiency and surface properties were systematically investigated. We found that the PL efficiency is solely related to the number of unpassivated surface Se atoms and, however, it is independent of the particle size. The exact mechanism of this size-independent behavior remains to be found.

Finally, we will state a conclusion in the last chapter of this thesis.

1.5 References

- 
- [1] L. E. Brus, J. Chem. Phys. **80**, 4403 (1984).
 - [2] Y. Wang and N. Herron, J. Phys. Chem. **95**, 525 (1991).
 - [3] C. B. Murray, D. J. Norris, and M. G. Bawendi, J. Am. Chem. Soc. **115**, 8706 (1993).
 - [4] P. Reiss, J. Bleuse, and A. Pron, Nano Lett. **2**, 781 (2002).
 - [5] D. V. Talapin, A. L. Rogach, A. Kornowski, M. Haase, and H. Weller, Nano Lett. **1**, 207 (2001).
 - [6] L. Manna, E. C. Scher, and A. P. Alivisatos, J. Am. Chem. Soc. **122**, 12700 (2000).
 - [7] Z. A. Peng and X. Peng, J. Am. Chem. Soc. **123**, 1389 (2001).
 - [8] V. L. Colvin, A. P. Alivisatos, and J. G. Tobin, Phys. Rev. Lett. **66**, 2786 (1991).
 - [9] P. Zhang and T. K. Sham, Phys. Rev. Lett. **90**, 245502 (2003).

- [10] H. Mattoussi, L. H. Radzilowski, B. O. Dabbousi, E. L. Thomas, M. G. Bawendi, and M. F. Rubner, *J. Appl. Phys.* **83**, 7965 (1998).
- [11] H. Borchert, D. V. Talapin, N. Gaponik, C. McGinley, S. Adam, A. Lobo, T. Moller, and H. Weller, *J. Phys. Chem. B* **107**, 9662 (2003).
- [12] J. Rockenberger, L. Troger, A. Kornowski, T. Vossmeier, A. Eychmuller, J. Feldhaus, and H. Weller, *J. Phys. Chem. B* **101**, 2691 (1997).
- [13] E. Rabani, B. Hetenyi, B. J. Berne, and L. E. Brus, *J. Chem. Phys.* **110**, 5355 (1999).
- [14] C. McGinley, M. Riedler, T. Moller, H. Borchert, S. Haubold, M. Haase, and H. Weller, *Phys. Rev. B* **65**, 245308 (2002).
- [15] M. C. Schlamp, X. G. Peng, and A. P. Alivisatos, *J. Appl. Phys.* **82**, 5837 (1997).
- [16] H. Mattoussi, L. H. Radzilowski, B. O. Dabbousi, E. L. Thomas, M. G. Bawendi, and M. F. Rubner, *J. Appl. Phys.* **83**, 7965 (1998).
- [17] M. Bruchez, M. Moronne, P. Gin, S. Weiss, and A. P. Alivisatos, *Science* **281**, 2013 (1998).
- [18] W. C. W. Chan and S. M. Nie, *Science* **281**, 2016 (1998).
- [19] Y. Yin, R. M. Rioux, C. K. Erdonmez, S. Hughes, G. A. Somorjai, and A. P. Alivisatos, *Science* **304**, p711 (2004).
- [20] R. D. Schaller and V. I. Klimov, *Phys. Rev. Lett.* **92**, 186601 (2004).
- [21] A. Trampert, O. Brandt, and K. H. Ploog, in *Crystal structure of group III Nitrides*, edited by J. I. Pankove and T. D. Moustakas, *Semiconductors and Semimetals* Vol., 50, (Academic, San Diego, 1998).
- [22] A. W. Stevenson and Z. Barnea, *Acta Cryst.* **B40**, 530 (1984).
- [23] C. Kittel, *Introduction to Solid State Physics* (John Wiley & Sons, 2005).

- [24] C. Y. Yeh, Z. W. Lu, S. Froyen, and A. Zunger, Phys. Rev. B **46**, 10086 (1992).
- [25] L. E. Brus, J. Chem. Phys. **79**, 5566 (1983).
- [26] F. Buda, J. Kohanoff, and M. Parrinello, Phys. Rev. Lett. **69**, 1272 (1992)
- [27] H. Fu and A. Zunger, Phys. Rev. B **55**, 1642 (1997).
- [28] A. Zunger, Phys. Rev. B **56**, 1496 (1997).
- [29] S. Sapra and D. D. Sarma, Phys. Rev. B **69**, 125304 (2004).
- [30] A. Tomasulo and M. V. Ramakrishna, J. Chem. Phys. **105**, 3612 (1996).
- [31] L. E. Brus, J. Phys. Chem. **90**, 2555 (1986).
- [32] Y. Kayanuma, Phys. Rev. B **38**, 9797 (1988).
- [33] L. W. Wang and A. Zunger, Phys. Rev. B **53**, 9579 (1996).
- [34] D. Brust, J. C. Phillips, and F. Bassani, Phys. Rev. Lett. **9**, 94 (1962).
- [35] J. Rockenberger, L. Troger, A. L. Rogach, M. Tischer, M. Grundmann, A. Eychmuller, and H. Weller, J. Chem. Phys. **108**, 7807 (1998).
- [36] S. H. Tolbert and A. P. Alivisatos, J. Chem. Phys. **102**, 4642 (1994).
- [37] R. W. Meulenberg, T. Jennings, and G. F. Strouse, Phys. Rev. B **70**, 235311 (2004).
- [38] V. L. Colvin, A. P. Alivisatos, and J. G. Tobin, Phys. Rev. Lett. **66**, 2786 (1991).
- [39] H. Hovel, B. Grimm, M. Pollmann, and B. Reihl, Phys. Rev. Lett. **81**, 4608 (1998).
- [40] M. Imamura and A. Tanaka, Phys. Rev. B **73**, 125409 (2006).
- [41] H. Borchert, D. V. Talapin, C. McGinley, S. Adam, A. Lobo, A. R. B. de Castro, T. Möller, and H. Weller, J. Chem. Phys. **119**, 1800 (2003).
- [42] J. Nanda and D. D. Sarma, J. Appl. Phys. **90**, 2504 (2001)

- [43] C. McGinley, M. Riedler, T. Möller, H. Borchert, S. Haubold, M. Haase, and H. Weller, *Phys. Rev. B* **65**, 245308 (2002).
- [44] H. Borchert, D. B. Talapin, N. Gaponik, C. McGinley, S. Adam, A. Lobo, T. Möller, and H. Weller, *J. Phys. Chem. B* **107**, 9662 (2003).
- [45] H. Borchert, S. Haubold, M. Haase, H. Weller, C. McGinley, M. Riedler, and T. Möller, *Nano Lett.* **2**, 151 (2002).
- [46] D. V. Talapin, A. L. Rogach, E. V. Shevchenko, A. Kornowski, M. Haase, H. Weller, *J. Am. Chem. Soc.* **124**, 5782 (2002).

